Mapping Disasters & Tracking Recovery in Conflict Zones Using Nighttime Lights

Zeal Shah*, Feng-Chi Hsu†, Christopher D. Elvidge†, Jay Taneja*
* *STIMA Lab, Department of Electrical and Computer Engineering, University of Massachusetts, Amherst*
† *Earth Observation Group, Payne Institute for Public Policy, Colorado School of Mines*

***Abstract*—The capability to map disasters and track recovery thereafter has seen substantial enhancement from the development of connected communication and imaging technology. In this work, we demonstrate a series of techniques for assessing the damage and the recovery process from the humanitarian crisis in Sana'a, Yemen. In particular, we make use of the Visible Infrared Imaging Radiometer (VIIRS) Day/Night Band (DNB), which produces nightly data on illumination levels globally at 750m resolution. While nearly all work that has previously been performed using the VIIRS DNB dataset uses monthly or annual composite data, we develop novel methods that leverage the nightly availability of this data source, particularly for mapping the scale and extents of illumination changes, accurately identifying the day when bombing occurred and illumination conditions changed, characterizing electricity outage patterns, and tracing the recovery of nighttime lighting both spatially and temporally. For each of these methods, we compare with publicly-available datasets to verify the accuracy of our observations. In total, these data, available only 1 day after an event, and the resulting analyses can be especially valuable for disaster response as well as targeting and tracking investments in recovery.**

I. Background

Yemen has been at the center of a humanitarian crisis since 2011 but the situation became more gruesome and violent in 2015 [4], [9]. Sana'a, the capital city of Yemen, controlled by the government, was captured by Houthi rebels in 2014 [9]. A series of events following Houthi capture of Sana'a led to Yemen's President Hadi leaving to Saudi Arabia, on March 25, 2015. Starting March 26, 2015, Saudi Arabia in coalition with Arab states launched airstrikes in Yemen against the Houthi rebel group, which have continued since then [4], [9]. Multiple cities including Sana'a have been the targets of airstrikes [9]. 1,658 airstrikes were reported in Sana'a spread over 570 days during the period of March 26, 2015, to May 29, 2019 [10]. Airstrikes have caused severe damage to infrastructure and substantial loss of human life in Yemen [4]. More than 10 million people were reported to be deprived of food, water, and healthcare in 2015, and by 2016, 21.2 million people needed humanitarian assistance in Yemen [9].

During such times of armed conflicts, it becomes very difficult and extremely dangerous to obtain ground information [18], so the use of satellite-based sensing has become a popular option to observe hard-to-reach areas especially in conflict zones [19]. Many researchers and international organizations have used daytime satellite images of conflict zones in Syria and Yemen to identify damaged structures in those areas [14], [20]. However, such approaches can be time-consuming and labor-intensive, and in time-critical situations, disaster response teams need immediate information regarding the impacted areas in order to plan an effective response [17]. To address this need, Facebook recently described a solution that uses their proprietary user location data to create near real-time crisis maps. These maps provide human mobility data to the responders during crisis [1]. However, these crisis maps are limited to tracking movements of people with the Facebook application installed on their smartphones and also contingent on the availability of cellular network services. Additionally, there are some crowdsourcing platforms like Ushahidi [32] that allow volunteers on the ground to mark locations and add disaster-related information in real-time. While this can be very useful, collecting the right data is likely to be challenging in conflict zones.

In this work, we examine the potential of high-frequency nightlights data to quickly and accurately assess the extent and depth of a crisis as well as monitor the recovery over time. Armed conflicts can cause severe damage to infrastructure which can cause power outages and also disrupt human activity in the region [4]. Multiple studies have shown that satellite observations of nighttime lights can be used to detect power outages [17], [22], and study the dynamics of human activity [24]. Nighttime lights (NL) data have been used for a variety of applications such as measuring grid reliability [25], tracking restoration efforts post natural disasters [23], estimating socioeconomic parameters [26], and most recently in tracking human activity during the COVID-19 pandemic [29]. There are two different sources of nighttime lights data available - the Defense Meteorological Satellite Program Operational Linescan System (DMSP-OLS) and Suomi National Polar-Orbiting Partnership Visible Infrared Imaging Radiometer Suite (NPP-VIIRS). NPP-VIIRS is the newer generation instrument with higher resolution, and has data publicly available starting from April 2012 in the form of monthly and annual NL composites [21]. Many of the previously conducted NL-based war studies - analysis of the Syrian crisis [27] and war between Russia and Georgia [28], used DMSP-OLS data. Only two studies [9], [18] have demonstrated evaluation of impact of war on a country using monthly VIIRS NL data.

This paper explores the potential of nightly VIIRS data instead of the monthly or annual composites from April 2012 to May 2019 to evaluate the spatio-temporal impact of war on the capital city of Yemen: Sana'a. Relative to monthly

data, the high temporal granularity (nightly) and timeliness of the nightly data are particular advantages. Relative to other sources of daytime imagery, the free availability of images, the consistency of coverage, and the ability to observe electric phenomena are the key advantages of VIIRS NL data. Using this unique data source, we propose a technique to produce near real-time, multi-dimensional, high-resolution disaster maps for the region to provide disaster managers with up-to-date information on the spatial extent of a disaster. We demonstrate identification of the precise date of a lighting event that can be matched with a disaster timeline. Further, we demonstrate the potential of nightly NL data to estimate the duration of outages on the ground and then propose two NL-based indicators for tracking recovery and restoration in a region. The intention of this study is not to assist with the ongoing recovery in Yemen, but rather to illustrate the potential of nightly NL data to be instrumental to response and recovery in future crises. In total, we demonstrate a series of disaster monitoring and recovery tracking capabilities that are enabled by NL data and we evaluate the agreement of our observations with public datasets where available. To provide a measure of ground truth to our techniques, we quantify the level of agreement between the best available public datasets and our damage assessment results. Where relevant datasets are not available or do not exist, such as for recovery estimation, we provide an intuitive validation that assesses our novel technique.

II. Data

A. Nighttime Lights

In this study, we use nighttime lights (NL) data recorded by the Visible Infrared Imaging Radiometer Suite (VIIRS) low light imaging Day/Night Band (DNB) on the NPP-Suomi satellite [21]. These data are provided with help from our collaborators in the Earth Observation Group (EOG) at the Payne Institute for Public Policy in Colorado School of Mines [33]. EOG processed the raw data recorded by VIIRS DNB at 750m resolution and provided it in form of a 15 arc-second grid for our study area. The study area covers two governorates of Yemen - Sana'a and Amanath Al Asimah, that we jointly refer to as the region of Sana'a for simplicity. Spatially, the NL grid of Sana'a is composed of 45 x 73 pixels with a pixel resolution of 15 arc-seconds ($\approx$ 450m) and the upper-left corner at 15◦31"N, 44◦7"E. Blue box in Figure 1 shows the boundary of NL grid for the region and the map inside the box represents our study area [11]. The data consists of nightly temporal profiles of radiance for every pixel in Sana'a from April 2012 to May 2019. The unit of radiance used in the dataset is $nW/sr/cm^2$. Radiance has been normalized for the satellite's scan angle effects beforehand and so is referred to as Nadir Normalized Radiance in the dataset. The monthly and annual composites available online are actually created by aggregating nightly scene collections. Figure 2 shows the variations in total nighttime lights (TNL) captured by annual, monthly and nightly composites of Sana'a. TNL is the sum

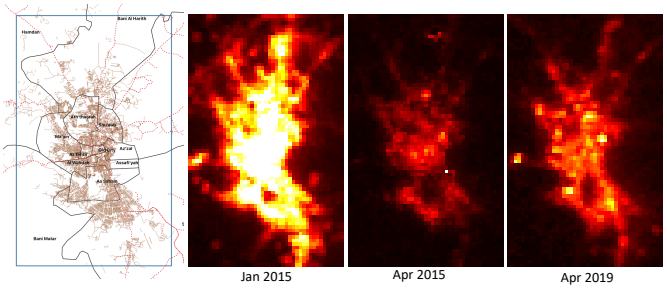

Fig. 1. Basemap of study area (area inside the blue box) is shown on the left [11]. Figures to the right of basemap are NL maps of Sana'a from Jan 2015, Apr 2015, and Apr 2019. Brighter pixels have high radiance and darker pixels have low radiance.

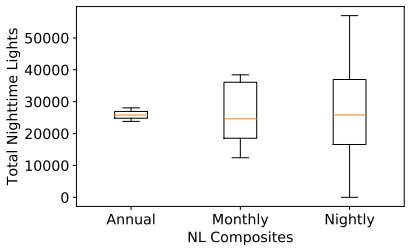

Fig. 2. Comparison of variation in total nighttime lights observed in annual, monthly, and nightly NL composites for Sana'a from Apr 2012 to Dec 2014

of radiance of all the pixels that lie inside a given region, providing a measure of total output rather than averaging output over a large area. For the given dataset, the range of TNL captured by annual and monthly composites is 7.44% and 45.63% of TNL range captured by nightly composites. By focusing on nightly data, we are able to observe more variation from place to place and day to day than we would otherwise, enabling a deeper look at the dynamics of this signal.

B. Auxiliary Data

1) Conflict Data: We use an openly available dataset of organized violence events in Yemen that has been geo-referenced, timestamped, and provided by the Uppsala Conflict Data Program (UCDP) [10], [11].

2) Infrastructure Data: Shapefiles for roads and streets, and locations of education and health sites in Yemen were acquired from the Humanitarian Data Exchange (HDX) platform [11]. The European Commission's Global Human Settlement (GHSL) data product called GHSL-BUILT was used to obtain built up presence data for Sana'a at a resolution of 30m [12].

3) Population Data: The GHSL-POP data product was used to acquire population distribution data for Sana'a at a resolution of 250m [13].

4) UNOSAT Data: UNITAR Operational Satellite Applications Programme (UNOSAT) identified 708 damaged structures in Sana'a by comparing daytime satellite images of Sana'a acquired on December 31, 2014, and May 15, 2015, locations of which have been made available online [14].

For every pixel, the NL dataset provides a bounding box representing bounds of a pixel. This allows us to associate an NL pixel with locations of education, health and UNOSAT

damaged sites that lie inside its bounding box, and with the shapefiles of roads that intersect with it. A bounding box can also be overlaid with GHSL datasets to compute population distribution and built-up area presence inside a pixel.

C. NL Data Pre-processing

NL data is often affected by lunar illuminance and cloud cover. The dataset contains flags that indicate whether a reading is affected by those factors. The usual technique to account for these factors is to filter out all the affected readings. However, this approach results in a loss of 51% of total coverage days for our locations, with 47% of days lost due to lunar-based filtering and 7% of days lost due to cloud-based filtering (we note that some days have both problems). To avoid losing observations from days with high lunar illuminance, we have implemented a seasonality correction mechanism that decomposes the unfiltered radiance signal of every pixel into three different components - trend, seasonality and residual - using Python's seasonal trend decomposition model available in the *statsmodels* package [16]. The seasonality component of low radiance signals clearly exhibited a presence of a 28-29 day repeating cycle indicating the considerable effect of lunar illuminance on those signals. Since no clear periodic pattern was observed in the seasonality component of high radiance signals, we applied correction to pixels with low radiance profiles only. For correction, we simply subtracted a signal's seasonal component from the original signal on high lunar days leaving radiance on low lunar days unchanged. Further, since cloud activity is not as periodic and predictable as lunar illumination, it poses a harder radiance correction challenge. For every pixel, we removed all the readings polluted by cloud cover which created missing timestamps in its nightly temporal profile. Assuming a linear trend, these gaps were then filled by linear interpolation of radiance between two consecutive cloud-free timestamps. We used this technique to create a spatially and temporally continuous dataset for the region.

III. Methodology

A. Baselines and Computation

We use two different pre-crisis baselines in this work - a baseline for disaster mapping and a baseline for recovery analysis. The pre-crisis period in this study is considered to be the period from April 1, 2012, to March 25, 2015, just prior to the commencement of airstrikes on Sana'a.

1) Baseline and Computation for Disaster Maps: The baseline dataset for disaster maps contains radiance data for all of the pixels on the same day-of-the-week for 20 weeks preceding the crisis. It takes into account the normally occurring daily and weekly radiance patterns and allows us to better differentiate between normal and abnormal changes in radiance on a specific day. To create a disaster map corresponding to a day of crisis, we collect the baseline data as stated and then calculate baseline mean and standard deviation for every pixel. Finally, we compare radiance on the day of crisis to the baseline statistics using z-score: $Z_p = (r_p - \mu_p)/(\sigma_p)$, where r_p, μ_p and σ_p denote crisis radiance, baseline mean, and baseline standard deviation for pixel p.

2) Baseline for Recovery Analysis: The baseline dataset for recovery analysis is composed of radiance values for all of the pixels from all days present in the pre-crisis period. It is more generic and provides an overview of radiance levels across the region not accounting for typical daily or weekly patterns.

B. Grouping Based on Pre-crisis (Baseline) Brightness

We used the baseline dataset discussed in Section III-A2, computed baseline mean, and then applied Jenk's Natural Breaks Classification algorithm to classify pixels into three groups based on their mean baseline brightness levels (μ_p) - Low ($\mu_p < 14$), Medium ($14 <= \mu_p < 42$), and High ($\mu_p >= 42$) [8]. Jenk's Natural Breaks Classification method creates clusters of similarly-valued pixels such that the variance within the clusters is minimized and the variance between the clusters is maximized [6], [7]. This grouping allows us to study the duration of outages and the rate of recovery experienced by pixels with different baseline brightness levels. High, medium, and low baseline brightness groups contained 19.6%, 62.2% and 18.2% of total built up area, respectively, and 47.2%, 44.7% and 8.1% of the total population, respectively.

C. Brief Study Overview

Airstrikes across Yemen during the period of March 26 to April 15, 2015, caused severe damage to electricity grids causing wide-spread blackouts in multiple regions including Sana'a [4], [9]. Figure 1 presents a snapshot of nighttime lights in Sana'a before the crisis (January 2015) and during two crisis timelines (April 2015 and April 2019). The impacts of airstrikes are clearly visible in the form of sharp drops in nighttime radiance across the region in April 2015. While the April 2019 snapshot shows that some magnitude of recovery has been achieved relative to April 2015, radiance levels have still not rebounded to pre-crisis levels.

IV. Disaster Maps

Disaster maps present statistics about changes in radiance associated with a region following a crisis relative to the pre-crisis baseline period [1]. We use z-score to highlight regions on a map with significant differences between their post-crisis radiance and typical radiance observed during the baseline.

In order to gauge a z-score value that would be reflective of real damage on the ground, we measured z-scores of NL pixels containing UNOSAT marked damaged sites. 708 reported damaged sites were linked to 198 NL pixels. Matching our analysis timeline with that of UNOSAT's, we computed z-scores between radiance values observed on May 15, 2015, and radiance values in baseline corresponding to December 31, 2014. 193 airstrikes were reported between December 31, 2014 and May 15, 2015, in Sana'a, causing radiance to drop all across the region [10]. But z-scores showed that pixels containing damaged sites experienced a more substantial drop in radiance (mean z-score = -2.3) relative to pixels that did not contain any damaged sites (mean z-score = -1.4). We believe

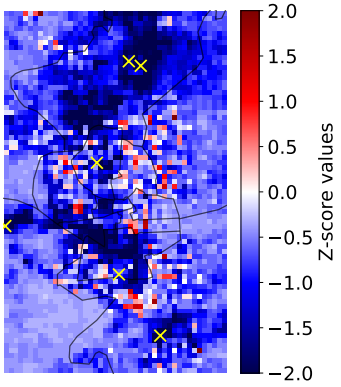

Fig. 3. Disaster map for Sana'a on March 26, 2015. Colorbar denotes z-score values, with darker colors indicating darkening of lights. Yellow markers show 6 bombing locations [10].

that this 64% additional reduction in radiance is a clue towards more significant airstrike activity in particular areas.

In this paper, we demonstrate disaster mapping for Sana'a following a series of 6 Saudi-led airstrikes on March 26, 2015 [10]. The disaster map as shown in Figure 3 was created by computing z-scores of radiance on March 26, 2015, for each pixel relative to its baseline. Z-scores were clipped between -2 and 2 for better visualization. Pixels with low z-scores (dark blue) represent severely impacted areas, which also closely align with regions surrounding the actual bombing locations (yellow markers) as reported by UCDP [10]. According to news reports [2], airstrikes in Sana'a following March 26, 2015, hit multiple different targets in the area for 15 minutes before departing. This indicates that the spatial extent of damage due to airstrikes was much larger than just a single location point or the areas close to that point. Our disaster map clearly captures this information - many more pixels were detected to have been impacted ($Z <= (-2)$) than just the ones near the bombing locations. Furthermore, we found that severely impacted pixels are at an average distance of 0.09 to 11.94 km from the marked bombing locations. Additionally, by filtering pixels based on low z-scores (($Z <= (-2)$), we were able to identify 4 more areas in Sana'a that had experienced direct/indirect impact of airstrikes - Maain, Al Wahdah, Hamdan and At Tahrir, in addition to the ones reported by UCDP - As Sabain, Aththaorah, Bani Al Harith, Bani Matar and Sanhan [10]. A key capability of this approach is that this detailed information on the extent of affected areas is available as soon as the very next day after the event.

For the task of infrastructure damage assessment, we classified NL pixels into 4 different damage categories based on their z-scores - severe decrease ($Z <= -2$), moderate decrease ($-2 < Z <= -1$), slight decrease ($-1 < Z < 0$) and increase ($Z > 0$). Reduction in lighting levels could be attributed to direct and indirect impact of airstrikes. Direct impact means loss of lighting due to direct damage to infrastructure present inside a pixel. Indirect impact to lighting can be in the form of power outages caused as a result of damage to electric grids. Spatially, 5.8%, 24.1%, and 65.1%

TABLE I
SUMMARY OF AREAS WITH DIFFERENT DAMAGE EXPERIENCES

Damage Group	Edu. sites (%)	Health sites (%)	Built-up (%)	Pop. (%)	TNL Change (%)
Severe	13.8	11.3	11.0	11.9	-87.4
Moderate	33.3	28.4	32.3	30.8	-64.5
Slight	39.7	47.8	41.5	43.0	-30.4
Increase	13.2	12.6	15.2	14.3	22.8

of the complete region experienced severe, moderate and slight impact, respectively. Severity of impact is also reflected in the TNL values of different groups before and after the airstrikes. TNL of groups that experienced severe, moderate, and slight impact, changed by -87.4%, -64.5% and -30.4%, respectively. Furthermore, 5.0% of total pixels exhibited an increase in radiance (TNL change of 22.8%) following the bombings, which based on our understanding may represent areas where people took temporary refuge following the crisis. Table I summarizes the proportion of infrastructure and population belonging to different damage groups. Such additional information can be very useful in creating an extensive list of structures, roads, and neighborhoods that possess a higher probability of having sustained damage due to airstrikes than others.

Potential Applications: While data in Table I coupled with structure locations do not provide a complete picture of the situation on the ground, they can serve as a good starting point for immediate planning of humanitarian response. We acknowledge that there is no adequate replacement for human intelligence in these types of situations, but we hope to augment that information with broader yet still detailed observations. The ability to create ad-hoc disaster maps within 24 hours of a crisis event and detect regions with a higher probability of containing damaged infrastructure at 15 arc-second spatial resolution can help the response teams in targeting their immediate response efforts and resources to severely impacted areas [1], [17]. Information regarding roads inside differently impacted pixels can help in selecting appropriate routes to send help to areas in need. Pixel-level hospital location data can help in coordinating with hospitals located in relatively less damaged areas beforehand for any medical needs. Further, quantities of resources like food and medicines can be estimated based on population values in each pixel.

V. CHANGE POINT DETECTION

Abrupt changes in a region's radiance can provide indirect information regarding different events on the ground like power outages and restoration, destruction and reconstruction of infrastructure, new electrification and construction, and more. In this section, we demonstrate that it is possible to identify exact dates of a loss-of-lighting event using nightly NL data and associate it with the disaster timeline to detect a possible cause for that event. Airstrikes in Sana'a beginning on March 26, 2015, impacted different sites at different times but the airstrikes specifically around April 12-13, 2015, severely damaged the electricity infrastructure, causing wide-spread blackouts [4]. Using this information as our reference, we

applied an offline change point detection algorithm on NL data from Sana'a to estimate dates when different sites were affected. This further emphasizes the capabilities that are possible with nightly observations.

Piece-wise linear regression available as a part of a Python package called *ruptures* was used to detect breakpoints in a signal that indicate abrupt changes in radiance [3]. Figure 4 shows sample detection outputs for 2 pixels that experienced a sudden drop in radiance on different dates - March 26, 2015, (sanaa_grid_10_11) and April 12, 2015 (sanaa_grid_8_28). Further, a second change point - a gradual and sustained growth in radiance - was detected in the pixel sanaa_grid_8_28 around June 4, 2016, following a long period of low lighting levels indicating radiance recovery.

Region-wide change point detection results summarized in Figure 5 show the proportion of pixels detected to have experienced a drastic reduction in radiance on a given date. Change points detected before March 26, 2015, closely matched with dates of remote violence acts as reported in the UCDP dataset, and a 100% of change points detected following March 25, 2015, coincided with dates of different airstrikes in the region [10]. Results indicate that 41.1% and 44.2% of the total pixels in Sana'a experienced abrupt drops in radiance during March 26-28 and April 12-15, 2015 periods, respectively. By April 15, 2015, lighting levels of 97.8% pixels had dropped drastically which coincides with the information that majority of regions had started experiencing blackouts due to severe damage to grid infrastructure [4]. Furthermore, a second change point was detected in the time series of 41% of the total pixels indicating onset of recovery. Recovery onset dates for different pixels ranged from June 2015 to April 2019 suggesting varying duration of low lighting periods experienced by different pixels after April 15, 2015. The remaining 59% of the pixels continued to experience low lighting and no detectable rise in radiance was found. These areas have yet to recover to their previous lighting levels.

Potential Applications: Usually the efforts to identify the exact date of damage caused to a site using daytime satellite images would require obtaining satellite images from the exact right times, which may be difficult. The nightly granularity and high spatial resolution of NL data can prove to be of great value in such cases. Detailed efforts like the UNOSAT damaged site identification can be complemented with nightly NL data that can allow observers to identify the damaged structures and also estimate the date of infliction for each one.

VI. Lighting Outages

As discussed in Section V, a significantly wider range of outage experiences were observed across the region after the blackouts caused by airstrikes on April 12-13, 2015. In this section, we show that nightly granularity of NL data can help us with estimating duration of lighting outages experienced by different pixels in Sana'a.

We define a lighting outage as an absence of detectable lighting levels on the ground on a night with low moon light and clear sky. A radiance value is classified as an outage if it

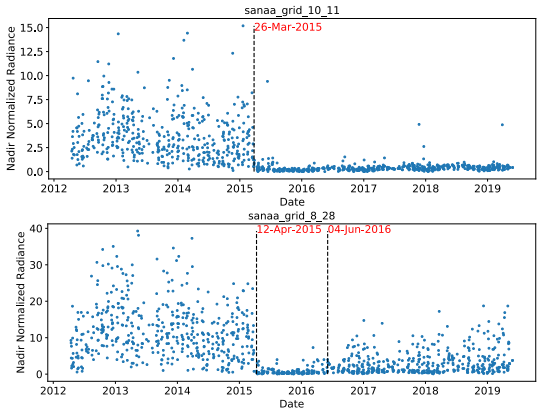

Fig. 4. Change point detection in the nightly NL profile of two pixels - sanaa_grid_10_11 (top) and sanaa_grid_8_28 (bottom).

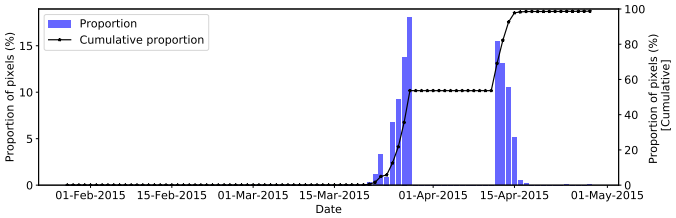

Fig. 5. Proportion of pixels with a detected "damage" change point on a given date between January 25, 2015, and May 1, 2015.

lies below a threshold of $1.0nW/sr/cm^2$ because the lighting levels below the threshold are difficult to detect by the satellite [21]. We quantify duration of lighting outages in form of a monthly outage rate which is calculated by dividing the total number of outages by total number of dark nights with clear sky in a given month. Figure 6 shows monthly outage rate for a single pixel from 2012 to 2019, which suddenly increased to 100% in April 2015, following which the pixel experienced a prolonged lighting outage for 30 months until October 2017.

To study the duration of lighting outages across the region, we computed average monthly outage rates experienced by a pixel in different baseline brightness groups as shown in Figure 7. Before April 2015, high and medium radiance pixels experienced less than 10% monthly outage rate indicating stable lighting levels while the low radiance pixel hit the threshold limit multiple times experiencing an outage rate of 30-60%. Monthly outage rates of high, medium, and low radiance pixels experienced a sharp increase from 0.26%, 2.58% and 57.28% in March 2015 to 42.78%, 71.60% and 97.72% in April 2015, respectively, as a result of damage inflicted on electric grids. Following April 2015, outage duration experienced by the high and medium radiance pixels has been decreasing steadily and their monthly outage rates have reached 1.6% and 16.6%, respectively. But monthly outage rate of a pixel in low radiance group has stayed between 95% and 100% following April 2015. Decrease in monthly outage rate doesn't imply growth of lighting levels but it implies their return to detectable levels indicating a possible rise in human activity.

Potential Applications: Technique to detect lighting outages

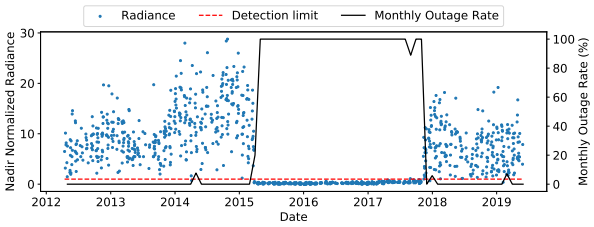

Fig. 6. Monthly outage rate of a single pixel in Sana'a plotted along its nightly NL profile and detection limit.

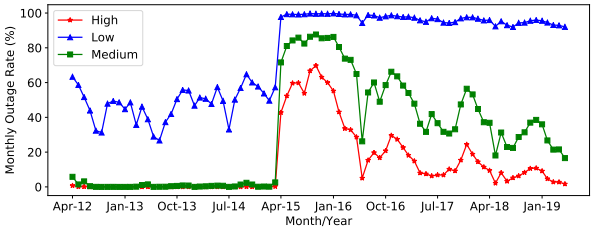

Fig. 7. Average monthly outage rate experienced by a pixel belonging to high, medium and low baseline brightness groups.

using NL data could be modified and applied to obtain electric grid reliability estimates from space [25]. It could be used for monitoring electric grids in the data-scarce, developing regions, where the grids are insufficiently monitored and highly unreliable [31]. The ability to estimate grid reliability using NL data can help utilities with power systems planning and maintenance and also help international development partners to monitor electric grid reliability independently from utilities.

VII. Tracking Recovery

Recovery is a long-term, spatially and temporally dynamic process that involves rebuilding, rehabilitating, and restoring a region following a disaster. Many different methods are used today to measure recovery - satellite image analysis, ground observations, surveys, and more [5]. In this section, we show that nightly NL data can also be leveraged to assess recovery. We propose two NL-based recovery indicators - the degree and rate of recovery - that can complement other recovery assessment studies. Again, we emphasize that these techniques are meant to augment human observations, not to replace them.

A. Degree of Recovery

Degree or magnitude of recovery is defined as the proportion of radiance that has been recovered at a given time relative to the baseline value. We compute degree of recovery on a monthly basis as the ratio of a pixel's average monthly radiance to its baseline mean. Figure 8 shows nightly NL data for a pixel in Sana'a that exhibited a steady rise in radiance starting June 4, 2016, following a 13 months long period of low lighting levels. Degree of recovery (red line) started at 25% in June 2016 and had reached 40% by May 2019.

Table II summarizes normalized TNL values for different baseline brightness groups from 2016 to 2019 along with the degree of recovery achieved by each in 2019. Normalized values were obtained by calculating mean TNL value for a

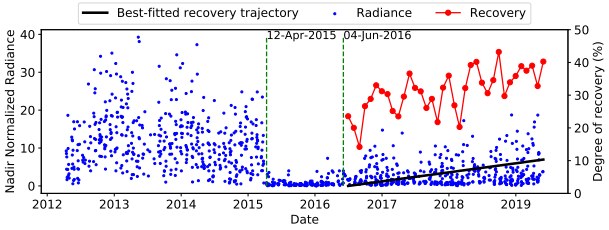

Fig. 8. Degree of recovery and best-fitted recovery trajectory of a single pixel in Sana'a plotted along its daily NL profile. Slope of trajectory is the pixel's rate of recovery ($0.198 nW/sr/cm^2/month$ which is approximately equal to 1.42% recovery/month relative to the baseline).

TABLE II
Recovery Summary of Groups with Different Baseline Brightness Levels

Baseline brightness	Normalized baseline TNL	Normalized TNL				Degree of recovery (%)
		2016	2017	2018	2019	
High	60.84	4.11	4.78	5.88	6.74	11.08
Medium	26.15	2.21	2.83	3.50	4.03	15.40
Low	3.14	0.64	0.83	0.88	0.82	26.23

group over the year and then dividing it by the total number of pixels in that group. Lighting levels for all the groups remained significantly low from 2016 to 2019. Normalized TNL values in 2016 for high and medium brightness groups were 6.8% and 8.4% of their respective baseline values, but the values continued to increase over time reaching 11.1% and 15.4% of their baseline levels in 2019, respectively. These readings indicate that human activities slowly continued to grow in the areas that were bright before and also presents a possibility of slight improvements in power supply over time. The lighting levels of the low radiance group remained below the detection threshold throughout the timeline, indicating no significant recovery. One particular shortcoming of degree of recovery as an indicator is that for low radiance pixels, even a slight change in the radiance can cause a significant increase or decrease in the indicator's value which can be misleading.

B. Rate of Recovery

Rate of recovery (ROR) is defined as the speed at which radiance levels rise over time. For a single pixel, ROR is the slope of line best fitted to its recovering radiance profile and is measured in radiance per month ($nW/sr/cm^2/month$). We apply linear regression to average monthly radiance values of a pixel's recovering profile to obtain the corresponding best fit line as shown in Figure 8. In order to visually investigate the spatial spread of ROR we created a rate of recovery map for Sana'a as shown in Figure 9. ROR in the region ranged from 0.019 to 0.82 but has been normalized between 0 and 1 for visualization purposes. Pixels with darker shades of blue exhibit negligible ROR while the pixels with red hue show pockets with high ROR. A majority of the high ROR pockets lie near and at the center of city indicating a relatively higher speed of recovery in urban areas. Additionally, Figure 9 shows that NL data allows us to study recovery at a spatial resolution considerably higher than that of administrative units.

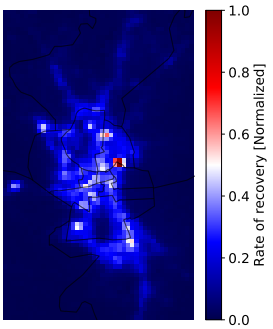

Fig. 9. Normalized rate of recovery (ROR) map of Sana'a.

TABLE III
PROPORTIONS OF BASELINE BRIGHTNESS GROUPS WITH DIFFERENT RATES OF RECOVERY (ROR)

Baseline brightness	Proportion of pixels (%)			Mean ROR[a]
	High ROR	Moderate ROR	Low ROR	
High	58.72	38.30	2.98	0.24
Medium	13.50	56.13	30.37	0.15
Low	0.04	1.73	98.23	0.04

[a] Unit of mean ROR is $nW/sr/cm^2/month$

To quantify the information presented in Figure 9, ROR values were classified into three different classes using Jenks natural breaks algorithm - low ($0.02 <= ROR < 0.09$), medium ($0.09 <= ROR < 0.22$) and high ($0.22 <= ROR < 0.89$) [6]. We then measured the proportion of pixels of each baseline brightness group belonging to different ROR classes as summarized in Table III. Mean ROR values in Table III illustrate the uneven speed of recovery across the region - pixels that had high baseline brightness are recovering at a higher rate (ROR=0.24), followed by pixels with medium (ROR=0.15) and low baseline brightness (ROR=0.04). 58.7% and 38.7% of pixels in the high brightness group are recovering at a high and medium rate respectively. Since a majority portion of the main city area was comprised of high brightness pixels pre-crisis, their ROR values match well with our visual observation that pockets with high ROR are concentrated inside the main city area. More than half (56.1%) of the medium brightness group appears to be recovering at a moderate pace while the low radiance areas do not show any signs of speedy recovery with 98.2% of them belonging to the low ROR class.

Potential Applications: NL data can provide a means to monitor the magnitude and speed of recovery across a region on a daily basis without physical intervention, which can augment sparse ground observations. Such information can potentially help governments and local stakeholders design and modify sectoral recovery strategies, monitor and evaluate progress of recovery, plan finances in a timely manner, and better manage relief funds from international organizations [5], [15]. Funding agencies that have invested in the re-development of the region can also track the progress of recovery process in a remote and independent manner.

VIII. TIME SERIES CLUSTERING

In this section, we are attempting to understand if spatial relationships among the NL patterns of adjacent clusters may provide insight into the interconnections between their infrastructure. To do this, we perform time series clustering on Sana'a's NL data to study the spatio-temporal evolution of clusters of pixels with similar temporal profiles over time. We extracted Sana'a's nightly NL data for three distinct periods: April 2012 - March 2015 (baseline), January - December 2016, and January - December 2018. Using NL data from a given period, a cross-correlation matrix was computed between temporal signals of all the pixels, which was then used as a distance matrix to perform hierarchical clustering in Python [30]. For every period, clustering output represents groups of pixels with highly correlated lighting signals. Clustering results have been summarized in Figure 10 and Table IV.

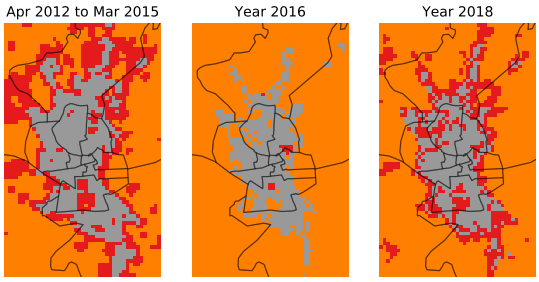

Fig. 10. Time series clustering outputs for three distinct periods - Apr 2012-Mar 2015 (left), Jan-Dec 2016 (center) and Jan-Dec 2018. (right). Gray, red, and orange colors represent urban, peri-urban and rural clusters, respectively.

We obtained 3 different clusters for the baseline period. Pixels in each cluster were contiguous and clearly represented a different part of Sana'a - urban, peri-urban, and rural, with TNL, population, and building density decreasing going from urban to rural. It shows that pixels belonging to a similarly developed environment exhibit high correlation in their lighting signals, indirectly indicating similarity in energy use and quality of grid power getting delivered. For the baseline period, the complete region consisted of pixels that are 25.9% urban, 25.8% peri-urban, and 48.2% rural pixels.

Clustering output for 2016 is representative of the spatial impact of airstrikes. 36.0% and 87.9% of the previously urban and peri-urban pixels, respectively, started exhibiting temporal behavior similar to the rural pixels, causing spatial growth of rural (by 1.66x), severe shrinking of peri-urban, and slight shrinking of urban clusters. So even though peri-urban areas had relatively higher population and total built-up area, their lighting dynamics closely resembled that of low-lit rural areas due to infliction of damage. But by 2018, the peri-urban cluster grew back significantly from 0.4% of the total region in 2016 to 18.0%. 16.9% of previously rural pixels joined the peri-urban region indicating possible growth, re-electrification, or electric grid repair in the periphery areas. Approximately 20% of the urban and 20% of the peri-urban pixels swapped their respective clusters indicating changes in lighting dynamics inside and near the periphery of the city. By 2018, the region still comprised of 64.4% rural pixels as compared to the baseline value of 48.2% which means the effect of damage still persisted in many urban and peri-urban areas.

TABLE IV
PROPORTION OF PIXELS BY CLUSTER TYPE DURING DIFFERENT PERIODS IN TIME

Cluster	Proportion of pixels (%)		
	2012-15	2016	2018
Urban	25.9	19.3	17.6
Peri-urban	25.8	0.4	18.0
Rural	48.2	80.3	64.4

IX. DISCUSSION

A. Limitations

Lunar correction mechanism used for correcting radiance data on high lunar days are rudimentary and must be improved for future studies. Data sources to verify many aspects of damage and recovery in crisis areas are typically very limited or unavailable. Significant changes in a region's NL values can be attributed to multiple factors on the ground, but it is not possible to identify the responsible factor using only NL data. Ground observations and daytime satellite images would be needed to make accurate inferences regarding the actual cause of changes in NL. Further, outage detection techniques will only be able to capture outages that occur or persist at the time of NPP-Suomi satellite's flyover.

B. Future Work

In the future, we plan on expanding the study to other major cities in Yemen using improved lunar correction and change point detection algorithms. Additionally, we aim to engage more directly with humanitarian professionals to better shape the outputs of this work for their utility.

X. CONCLUSION

In this work, we demonstrated a series of novel capabilities for disaster mapping and recovery tracking after a crisis, each enabled by the heretofore unexplored nightly VIIRS DNB dataset. We analyzed the humanitarian crisis that has been unfolding in Yemen over the last decade, with particular focus on the ramp up of airstrikes in March and April of 2015 as well as the long recovery that continues to this day. Our new methods can assess the scale and scope of disasters as well as trace the arduous and uneven process of recovery at a heretofore unprecedented level of detail. We believe that these capabilities can be valuable in a wide array of humanitarian and economic crises, providing guidance for fast and targeted response as soon as one day after the crisis begins.

REFERENCES

[1] P. Maas, S. Iyer, A. Gros, W. Park, L. McGorman, C. Nayak, and A. Dow, "Facebook disaster maps: Aggregate insights for crisis response & recovery," Proceedings of the 16th ISCRAM Conference, Spain 2019.

[2] Y. Taha, "Yemen conflict: Residents in Sana'a facing 'worst days of slow death' as air strikes continue," ABC News, April 2015.

[3] C. Truong, L. Oudre, and N. Vayatis, "Selective review of offline change point detection methods," Signal Processing, 167:107299, 2020.

[4] J. Dalek, R. Deibert, S. McKune, P. Gill, N. Noor, and A.Senft, "Information controls during military operations: The case of Yemen during the 2015 political and armed conflict".

[5] D. Contreras, G. Forino, and T. Blaschke, "Measuring the progress of a recovery process after an earthquake: the case of L'aquila, Italy", International Journal of Disaster Risk Reduction, 2017.

[6] G. Jenks, "The Data Model Concept in Statistical Mapping", International Yearbook of Cartography 7, 1967.

[7] R. Monteiro, V. Pereira, and H.G. Costa, "A Multicriteria Approach to the Human Development Index Classification," Soc Indic Res 136, 2018.

[8] Python implementation of Jenk's Natural Breaks Classification. https://github.com/mthh/jenkspy

[9] W. Jiang, G. He, T. Long, and H. Liu, "Ongoing conflict makes Yemen dark: From the perspective of nighttime light", Remote Sensing, 2017.

[10] R. Sundberg, and E. Melander, "Introducing the UCDP Georeferenced Event Dataset", Journal of Peace Research, vol.50, no.4, 523-532, 2013.

[11] The Humanitarian Data Exchange Platform. https://data.humdata.org/organization/hdx.

[12] C. Corbane, A. Florczyk, M. Pesaresi, P. Politis, and V. Syrris, "GHS built-up grid, derived from Landsat, multitemporal (1975-1990-2000-2014), R2018A," European Commission, Joint Research Centre.

[13] M. Schiavina, S. Freire, and K. MacManus, "GHS population grid multitemporal (1975, 1990, 2000, 2015) R2019A," European Commission, Joint Research Centre.

[14] UNITAR-UNOSAT, "Damage assessment of Sana'a city, Sana'a governorate, Yemen", June 2015.

[15] United Nations Development Programme, "A guidance note: National post-disaster recovery planning and coordination", May 2017.

[16] R. Cleveland, W. Cleveland, J. McRae, and I. Terpenning "STL: A Seasonal-Trend Decomposition Procedure Based on LOESS," Journal of Official Statistics, 6, 1990.

[17] C. Aubrecht, C. Elvidge, D. Ziskin, K. Baugh, B. Tuttle, E. Erwin & N. Kerle, "Observing power blackouts from space - A disaster related study," 2009.

[18] X. Li, R. Zhang, C.Q. Huang, D.R. Li, "Detecting 2014 northern Iraq insurgency using nighttime light imagery," Int. J. Remote Sens. 36, 2015.

[19] F.D.W. Witmer, "Remote sensing of violent conflict: Eyes from above," Int. J. Remote Sens. 2015, 36, 2326–2352.

[20] A. Marx, "Detecting urban destruction in Syria: A Landsat-based approach," Remote Sensing Applications: Soc and Env, 4, 2016.

[21] C. Elvidge, K. Baugh, M. Zhizhin, F.C. Hsu, T. Ghosh, "VIIRS nighttime lights," International Journal of Remote Sensing, 38:21, 2017.

[22] C. Cao, X. Shao & S. Uprety, "Detecting light outages after severe storms using the S-NPP/VIIRS day/night band radiances," Geoscience and Remote Sensing Letters, IEEE, 10, 2013.

[23] T. Gillespie, E. Frankenberg, K.F. Chum, D. Thomas, "Nighttime lights time series of tsunami damage, recovery, and economic metrics in Sumatra, Indonesia," Remote Sens Lett., January 2014.

[24] C. Elvidge, P. Cinzano, D.R. Pettit, J. Arvesen, P. Sutton, C. Small, R. Nemani, T. Longcore, C. Rich, J. Safran, et al., "The nightsat mission concept," Int. J. Remote Sens, 28, 2007.

[25] M. Mann, E.K. Melaas, A. Malik, "Using VIIRS Day/Night Band to Measure Electricity Supply Reliability: Preliminary Results from Maharashtra, India,"Remote Sens., 8, 2016.

[26] C. Elvidge, P.C. Sutton, T. Ghosh, B.T. Tuttle, K. Baugh, B. Bhaduri, E. Bright, "A global poverty map derived from satellite data," Comp. Geosci. 35, 2009.

[27] X. Li, D. Li, "Can nighttime light images play a role in evaluating the Syrian crisis?," Int. J. Remote Sens. 2014, 35, 6648–6661.

[28] F. Witmer & J. O'Loughlin, "Detecting the effects of wars in the caucasus regions of Russia and Georgia using radiometrically normalized DMSP-OLS nighttime lights imagery," GISci. Remote Sens. 2011.

[29] C. Elvidge, F. Hsu, T. Ghosh, M. Zhizhin, "World Tour of COVID-19 Impacts on Nighttime Lights", 2020.

[30] Python Scipy heirarchical clustering. https://docs.scipy.org/doc/scipy/reference/cluster.hierarchy.html

[31] S. Correa, N. Klugman, J.Taneja, "How Many Smartphones Does It Take To Detect A PowerOutage?", Proceedings of the ACM e-Energy Conference, Germany, 2018.

[32] O. Okolloh, "Ushahidi, or 'testimony':Web 2.0 tools for crowdsourcing crisis information," Participatory Learning and Action 59, 2009.

[33] Earth Observation Group, the Payne Institute for Public Policy, Colorado School of Mines. https://payneinstitute.mines.edu/eog